LAWRENCE
LIVERMORE
NATIONAL
LABORATORY

LLNL-JRNL-771042

Frequency-to-Time Optical Arbitrary Waveform Generator

D. E. Mittelberger, R. Muir, M. Hamamoto, M. Prantil, J. Heebner

April 2, 2019

Optics Letters

Disclaimer

Frequency-to-Time Optical Arbitrary Waveform Generator

D. E. Mittelberger[1,*], R. D. Muir[1], M. Y. Hamamoto[1], M. A. Prantil[1], and J. E. Heebner[1]

[1] Lawrence Livermore National Laboratory, 7000 East Ave., Livermore, CA, 94550, USA
[*] Corresponding author: mittelberger1@llnl.gov

Received 4 April 2019; accepted 25 April 2019; posted 3 May 2019 (Doc. ID 364244); published 30 May 2019

We introduce a novel optical arbitrary waveform generator that can create transform-limited ps-scale features over long (>300 ps) records. This has potential applications for controlling and/or mitigating laser-plasma interactions, laser machining, and studies of molecular dynamics. The technique works by patterning the spectrum of a short pulse and optically transforming this spectral pattern to the time domain via a $\chi^{(2)}$-based frequency-to-time converter. We derive the theory of operation and present experimental results demonstrating 4 ps resolution and 330 ps record length.

https://doi.org/10.1364/OL.44.002863

Many optical arbitrary waveform generation (AWG) techniques have been demonstrated across various timescales. Electro-optical Mach-Zehnder modulators driven by electrical arbitrary waveform generators can achieve near arbitrary record lengths but are limited by electron transport to coarse (∼100 ps) temporal resolution. Spectral pulse shapers [1, 2] and acousto-optical filters [3, 4] have achieved the finest resolutions but do not scale well to long record length due to spectral resolution demands. Pulse train replicators [5, 6] have simultaneously achieved fine resolution and long records but only with a limited number of replicated features. A simpler alternative to these methods is chirped pulse spectral shaping [7, 8], often referred to as frequency-time conversion. It can achieve long record lengths, limited only by how long a dispersed pulse can be made, but its resolution falls far short of the transform limit. Moreover, this technique results in a chirped output, which is undesirable for many applications. To our knowledge, no method exists that can generate long (>300 ps) record lengths with fine (ps-scale) transform-limited features.

In the related research of optical recorders, a variety of techniques have been developed to measure optical waveforms with record and resolution limits that have greatly surpassed the limits of AWG [9]. Nonlinear optical time-to-frequency converters [10–12] in particular can measure waveforms with >200 ps record length and <1 ps resolution [13]. The inverse of this technique, frequency-to-time conversion, is capable of generating optical arbitrary waveforms with similar length and resolution. In this Letter, we demonstrate a novel mechanism of nonlinear optical frequency-to-time conversion, termed Spectrally Transcribed And Chirp-Corrected Arbitrary Temporal Optimizer (STACCATO), and show that it can be used to generate arbitrary temporal waveforms that are a direct scaling of the patterns applied in the spectral domain.

The STACCATO system combines an arbitrary spectral filter (*e.g.* a spectral shaper) and a frequency-to-time converter to optically transform the spectral pattern into the time domain, creating an unchirped pulse with an arbitrary temporal profile. This method is distinct from chirped pulse spectral shaping, which leaves the pulse chirped and unfocused in time. The converter consists of two equal-magnitude dispersive elements surrounding a $\chi^{(2)}$-based time lens. The time lens is an optical parametric amplifier (OPA) operated as a difference frequency generator, where the OPA pump frequency and chirp are prescribed such that the system output is at the same wavelength as the input laser pulse and emerges unchirped. STACCATO is related to temporal imaging that can magnify waveforms in

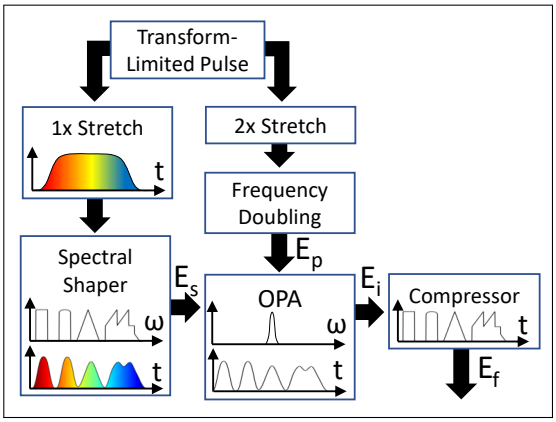

Fig. 1. Schematic of STACCATO system. One copy of the input pulse is stretched and spectrally shaped to create the OPA signal, E_s. The other copy is stretched twice as much and frequency doubled to create the pump, E_p. An OPA generates an idler, E_i, at the pump-signal difference frequency. The idler is narrowband because the signal and pump chirps cancel out. Finally, the idler is sent through a compressor to sharpen the temporal profile. Spectrum and intensity are shown at key stages, with chirp indicated by a color gradient. The key feature of this process is that the output temporal profile is an unchirped scaled replica of the patterned signal spectrum.

time [14–17], which allows fast temporal features to be measured with slow diagnostics. Temporal imaging has also been used to convert slow arbitrary waveforms to ps-scale resolution [18]. Here, the spatial analogue of STACCATO is not an imaging system but rather a Fourier optical transformer [19, 20].

An overview of the STACCATO concept is shown in Fig. 1. A transform-limited input pulse, *e.g.* from a mode-locked oscillator, is stretched and spectrally patterned via a programmable filter (*e.g.* a spectral shaper) to create a signal pulse, E_s. The spectral profile imposed on the signal is the desired temporal profile with time mapped to frequency. Next, an OPA creates an idler, E_i, at the difference frequency between the signal pulse and a chirped pump pulse. The pump, E_p, originates as a synchronized copy of the transform-limited pulse, stretched twice as much as the signal pulse and then frequency doubled so the idler has the same center frequency as the input. The dispersion of the signal and pump must be of the same sign because the idler field is proportional to the product of the pump field and the complex conjugate of the signal field. Further, for the signal and pump chirp to be equal in order to properly cancel in the OPA, the pump must have twice dispersion (half the chirp) as the signal prior to frequency doubling. Finally, a compressor adds dispersion to the idler which sharpens, or temporally focuses, the idler's time domain profile into a scaled replica, E_f, of the frequency-domain signal pattern. Unlike most time lens embodiments, the two dispersive elements in the system surrounding the time lens must have opposite signs because the idler continues on as the phase conjugate of the signal.

The STACCATO setup is similar to that of Ref. [19] with three key differences. 1) This system implements a true spectral shaper, as opposed to using a spatial mask in the compressor which cannot provide fine spectral resolution. 2) The spectral shaping occurs on the signal of the OPA rather than on the pump, and thus errors in the produced temporal profile are linearly, rather than exponentially, proportional to errors in the spectral patterning. 3) The addition of the final compressor is capable of dramatically improving the temporal resolution from $2(2\ln(2)\phi_2)^{1/2}$ to the transform limit $4\ln(2)/\Delta\omega$, where ϕ_2 is the group delay dispersion (GDD) of the stretcher and $\Delta\omega$ is the full width at half maximum (FWHM) spectral bandwidth. For our parameters, this is a factor of $\sim 35\times$ improvement.

To see explicitly that the temporal profile of the STACCATO output pulse is the spectral profile imposed by the spectral shaper, first suppose that the stretched, spectrally patterned signal pulse is given by

$$E_s(t) = \mathfrak{F}^{-1}\left\{\tilde{A}_s(\omega)e^{\frac{i}{2}\phi_2(\omega-\omega_0)^2}\right\} = A_s(t)e^{-i\omega_0 t}e^{\frac{-i}{2}t^2/\phi_2} \quad (1)$$

where $\mathfrak{F}$ indicates a Fourier transform, ϕ_2 is the group delay dispersion imparted by the stretcher, and $\tilde{A}_s(\omega)$ is the patterned spectral envelope. This signal is unsatisfactory as an arbitrary waveform for two reasons: 1) it is chirped and 2) the temporal features in $A_s(t)$ are not as sharp as a transform-limited feature because stretching reduces the local bandwidth. Next, the frequency-doubled pump is given by

$$E_p(t) = \left[A_p(t)e^{-i\omega_0 t}e^{\frac{-i}{2}t^2/(2\phi_2)}\right]^2 = A_p^2(t)e^{-i2\omega_0 t}e^{\frac{-i}{2}t^2/\phi_2} \quad (2)$$

where it should be noted that the pump (prior to frequency doubling) has twice the GDD of the signal and therefore half the chirp (instantaneous frequency *vs.* time). Frequency doubling creates a pump pulse with the same slope of $1/\phi_2$. The OPA then cancels the chirp through difference frequency generation of an idler, proportional to

$$E_i(t) \propto E_p(t)E_s^*(t) = A_s^*(t)e^{-i\omega_0 t}. \quad (3)$$

For simplicity, we assume that the frequency-doubled pump pulse profile is flat ($A_p^2(t) \approx 1$ for the duration of the signal pulse). The flat-top condition is equivalent to the pump spectrum being flat since the pulse is highly stretched.

The idler acquires the intensity profile of the stretched signal and the quadratic temporal phase of the pump. This cancels the signal chirp, but the residual quadratic spectral phase requires a final compressor to sharpen fine temporal features to the transform limit. The field after the compressor is related to the idler spectrum by

$$\begin{aligned} E_f(t) &= \mathfrak{F}^{-1}\left\{\mathfrak{F}\left\{E_i(t)\right\}e^{-\frac{i}{2}\phi_2(\omega-\omega_0)^2}\right\} \\ &\propto \tilde{A}_s^*(t/\phi_2+\omega_0)e^{-i\omega_0 t}. \end{aligned} \quad (4)$$

The final temporal profile is thus a scaled complex conjugate of the spectral profile of the signal.

The above derivation assumed $A_p^2(t) \approx 1$, but a finite pump duration leads to a finite temporal resolution. If the pump is a Gaussian with FWHM duration τ before frequency doubling, then including this factor in Eq. (2) yields a final electric field that is the pattern convolved with an impulse response function

$$\begin{aligned} E_f(t) \propto\ & e^{\frac{i}{2}t^2/\phi_2}e^{-i\omega_0 t} \\ & \times \int \tilde{A}_s^*(\omega)e^{\frac{-i}{2}\phi_2(\omega-\omega_0)^2}e^{-\frac{\tau^2}{16\ln(2)}(\omega-\omega_0-t/\phi_2)^2}d\omega. \end{aligned} \quad (5)$$

The intensity of this electric field has a minimum FWHM duration (the temporal resolution) of $\tau_{min} = 4\sqrt{2}\ln(2)\phi_2/\tau$. If instead the pump is a flat top or high-order super-Gaussian of FWHM τ, the final electric field is given by

$$\begin{aligned} E_f(t) \propto\ & e^{\frac{i}{2}t^2/\phi_2}e^{-i\omega_0 t} \\ & \times \int \tilde{A}_s^*(\omega)e^{\frac{-i}{2}\phi_2(\omega-\omega_0)^2}\mathrm{sinc}\left[\frac{\tau}{2}(t/\phi_2-(\omega-\omega_0))\right]d\omega. \end{aligned} \quad (6)$$

The associated intensity has a minimum FWHM duration of $\tau_{min} = 2.78...\times 2\phi_2/\tau$. In both cases, the pump has a FWHM duration $\tau = 2\phi_2\Delta\omega$ before frequency doubling, where $\Delta\omega$ is the spectrum FWHM width of the input pulse (before doubling). The minimum FWHM feature size is thus

$$\tau_{min} \approx \begin{cases} 1.96/\Delta\omega & \text{Gaussian} \\ 2.78/\Delta\omega & \text{Flat Top} \end{cases} \quad (7)$$

which corresponds to a monochromatic signal $\tilde{A}_s(\omega) = \delta(\omega-\omega_0)$ at the spectral shaper output. In both cases, STACCATO is capable of achieving a temporal resolution slightly better than the transform limit of the input pulse ($4\ln(2)/\Delta\omega \approx 2.77/\Delta\omega$).

To experimentally verify the STACCATO concept, we built a testbed (shown in Fig. 2) at the Lawrence Livermore National Laboratory. The input pulse is derived from an oscillator (Lumentum GLX-200) with a 6 nm FWHM spectrum centered at 1053 nm. This pulse propagates through a Martinez stretcher [21] with design GDD = 36.7 ps^2/rad and two copies are made. Amplification of both copies to a few mJ is necessary so that the signal strength of the idler is sufficient to be measured with an autocorrelator. One copy is immediately amplified, resulting in

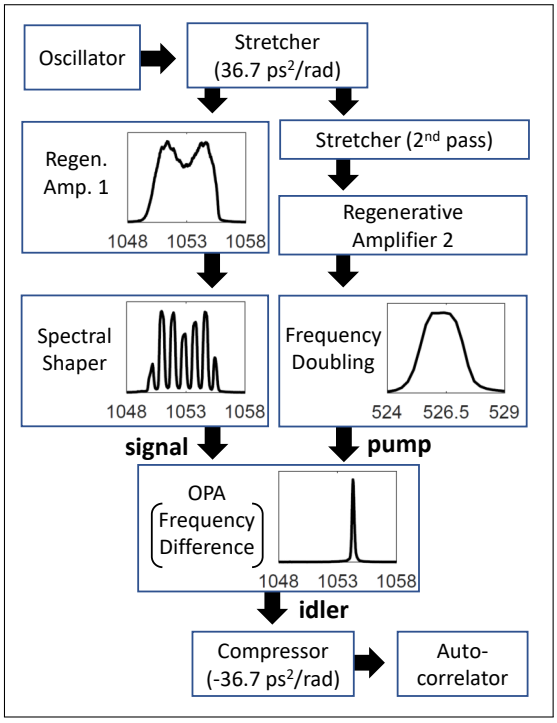

Fig. 2. Experimental setup. A transform-limited pulse from an oscillator is stretched and two copies are made. One copy is amplified and spectrally shaped to become the OPA signal. The other is passed through the stretcher again, amplified, and frequency doubled to create the OPA pump. The frequency-differencing OPA creates an idler that is passed through a final compressor to generate the desired temporal profile. The result is measured with a scanning autocorrelator. Measured spectra (normalized to unity) after key stages are plotted.

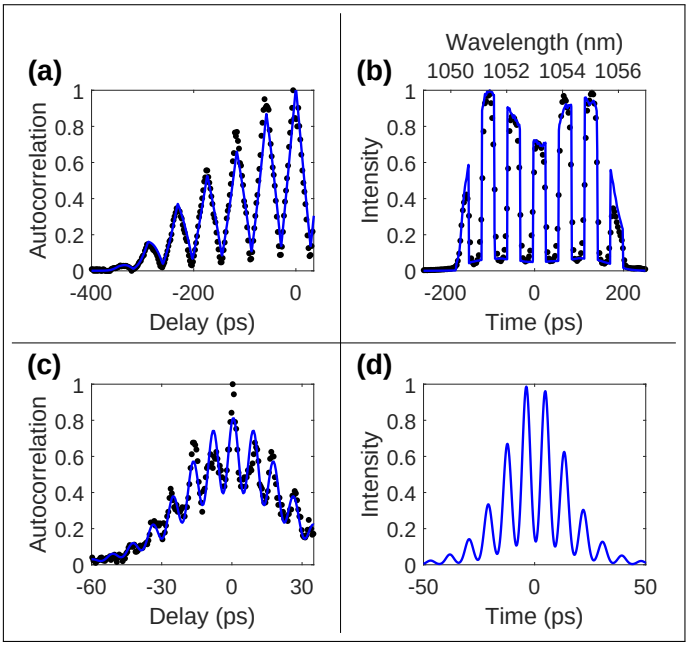

Fig. 3. Normalized autocorrelations and corresponding temporal profiles. (a) Measured (black points) and matching calculated (blue) autocorrelations with long record and coarse features. (b) Measured (black points) and calculated (blue) signal spectrum, plotted against wavelength and scaled time $t = \phi_2(\omega - \omega_0)$. (c) Measured (black points) and matching fit (blue) autocorrelations with short record/fine temporal features. (d) Temporal profile fit to measured autocorrelation.

a 330 ps long pulse with 5 nm FWHM of bandwidth (see Fig. 2 inset) due to gain narrowing in the regenerative amplifier. The pulse is then spectrally shaped with a home-built spectral shaper with a ~0.9 nm/mm mapping [1] to create the OPA signal pulse. The other copy (the pump) goes through the stretcher a second time before being amplified and frequency doubled to 526.5 nm in a 3 mm thick LBO crystal. An intracavity birefringent filter is used to achieve a flat-top spectrum (see Fig. 2 inset), which satisfies $A_p(t) \approx 1$. The signal and frequency-doubled pump are combined in an OPA oriented for difference frequency generation using a 2 cm thick LBO crystal. The generated idler is then temporally sharpened in a Treacy compressor [22] with GDD = -36.7 ps^2/rad and measured via a scanning autocorrelator.

In order to test the STACCATO concept, two spectral patterns were imposed: a coarse pattern to demonstrate record length and a fine pattern to demonstrate temporal resolution. In the first, a uniform comb mask (line width 500 μm) was used in the spectral shaper to create a regular pattern of flat-topped peaks of width ~0.5 nm (corresponding to temporal features of ~30 ps). The results are shown in the top row of Fig. 3. The measured autocorrelation (black points) of the coarse pattern is plotted in Fig. 3(a), which shows the 330 ps long FWHM record length of the generated optical waveform. Figure 3(b) shows the corresponding measured spectrum, which is also the expected temporal profile with the scaling $t = \phi_2(\omega - \omega_0)$. The spectrum pedestal is due to the non-zero reflectivity (R ~4%) of the gaps in the chrome-on-glass mask (R ~60%). Sharp spectral features are blurred due to the 0.1 nm resolution of the spectrometer (OceanOptics HR4000) so the autocorrelation of the measured spectrum has much lower contrast than the measured autocorrelation. A hypothesized spectrum/temporal profile (Fig. 3(b) blue line) was calculated from the unmodulated spectrum (Fig. 2 inset) and the reflectivities given above, which shares the approximate amplitude, peak spacing and width of the measured spectrum. Its autocorrelation (Fig. 3(a) blue line) agrees well with measurements, so we believe it is a good representation of the actual temporal profile. Deconvolution of the measured spectrum gave similar results with significant noise.

To demonstrate the generation of fine temporal features, a second comb mask (line width 75 μm) and an 0.5 nm bandpass filter were used in the spectral shaper. The record length was intentionally truncated from >300 ps to 50 ps using the bandpass filter to limit the number of features and improve the contrast of the autocorrelation. The measured autocorrelation is shown in Fig. 3(c) as black points and demonstrates a resolvable feature size of 4 ps, assuming Gaussian features. This is in agreement with simulations that predict a feature size of 4-5 ps for a 75 μm line width. The corresponding spectral features were smaller than the 0.1 nm spectrometer resolution, so the temporal profile was determined by a parameterized fit to the autocorrelation. The fit function was a series of Gaussians with an envelope that matched the measured spectrum. The resulting temporal profile is shown in Fig. 3(d) and the corresponding autocorrelation is plotted in blue in Fig. 3(c). The temporal features are Gaussian, rather than flat-topped as in Fig. 3(b), because of the spectral shaper resolution.

The STACCATO system also enables direct control of the

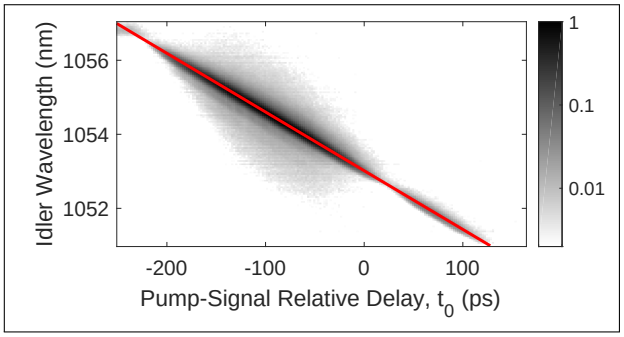

Fig. 4. Dependence of idler spectrum (grayscale, normalized spectrometer counts) on delay between the pump and signal pulses. Linear best fit is plotted in red.

output carrier frequency. Adding a time delay $t \rightarrow t - t_0$ between the signal and pump in Eq. (1) and substituting into Eq. (3) shows that the peak of the output spectrum can be shifted by $\Delta\omega = t_0/\phi_2$, as in [23]. In Fig. 4, the measured idler spectra are plotted against the pump-signal delay (zero point set at 1053 nm), along with an intensity-weighted linear fit (red). The (inverse of the) fit slope is -62.7 ± 0.4 ps/nm, corresponding to a GDD of 37 ± 0.2 ps^2/rad. The uncertainty results from the threshold (2%-20% of maximum) applied before the fit.

We described and demonstrated a novel optical AWG for creating arbitrary laser temporal profiles. Based on the theory developed above (Eq. (4) and Eq. (7)), the STACCATO method is capable of creating transform-limited features (<1 ps) over stretchable pulse lengths (>1 ns). Potential applications are the control and/or mitigation of laser-plasma interactions (*i.e.*, STUD pulses [24, 25]), high-energy-density experiments, laser machining [26], and studies of molecular dynamics [27].

An important figure of merit for AWGs is the number of resolvable temporal features. For STACCATO, the dispersion of the signal and pump changes the record length without affecting the temporal resolution (see Eq. (7), from which $N_{resolvable} = \tau_{signal}/\tau_{min} \propto \phi_2$). Practically, the number of resolvable spots is limited by achievable stretcher/compressor dispersion and spectral shaper resolution, but there is no fundamental upper limit. The described testbed demonstrated a 330 ps record and 4 ps resolution, which implies ~80 resolvable features although this is impractical to demonstrate with an autocorrelator. The capability of the STACCATO frequency-to-time converter to practically scale to >250 resolvable spots is supported by the time-to-frequency converter demonstrated by Ref. [13].

The use of a spatial light modulator (SLM) in place of static masks in the spectral shaper would create a system with a programmable temporal pattern. Only the amplitude need be specified to achieve a transform-limited intensity profile. Additionally, a spectral phase shift imposed at the mask would be transformed directly to temporal phase, creating an arbitrary instantaneous frequency *vs.* time. This system could be made considerably more robust by combining it with a single-shot temporal characterization system, such as SLIDER [28] or SLICER [29], and performing iterative optimization with the SLM to correct for non-idealities in the system (*e.g.* non-uniform pump temporal profile A_p). Because the mapping of spectrum to time is one-to-one, closed-loop operation should be possible without a look-up table.

The STACCATO method offers several advantages over alternative optical AWG techniques. In particular, it is a direct method of temporal patterning (*i.e.*, the mapping from the spectrum to time is linear and one-to-one), as opposed to traditional spectral pulse shaping in which both the Fourier transform's amplitude and phase must be specified. It also allows control of the central frequency by varying the delay between the pump and signal pulses and should also allow control of the instantaneous frequency via a phase modulating SLM. STACCATO thus introduces a novel capability for transform-limited optical arbitrary waveform generation over long (>300 ps) record lengths.

Funding. U.S. Department of Energy (DE-AC52-07NA27344); Lawrence Livermore National Laboratory (LLNL).

Acknowledgment. We wish to acknowledge Bedros Afeyan for providing motivation for this concept and its applications. We also wish to acknowledge Abe Handler, Tracy Budge, and Mila Novikova who helped build the subsystems and hardware.

REFERENCES

1. J. P. Heritage, A. M. Weiner, and R. N. Thurston, Opt. Lett. **10**, 609 (1985).
2. S. T. Cundiff and A. M. Weiner, Nat. Photonics **4**, 760 (2010).
3. P. Tournois, Opt. Commun. **140**, 245 (1997).
4. F. Verluise, V. Laude, J.-P. Huignard, P. Tournois, and A. Migus, J. Opt. Soc. Am. Part B **17**, 138 (2000).
5. C. W. Siders, J. L. W. Siders, A. J. Taylor, S.-G. Park, and A. M. Weiner, Appl. Opt. **37**, 5302 (1998).
6. W. R. Donaldson, J. R. Marciante, and R. G. Roides, IEEE J. Quantum Electron. **46**, 191 (2010).
7. J. Azaña and L. R. Chen, J. Opt. Soc. Am. B **19**, 2758 (2002).
8. I. S. Lin, J. D. McKinney, and A. M. Weiner, IEEE Microw. Wirel. Compon. Lett. **15**, 226 (2005).
9. I. A. Walmsley and C. Dorrer, Adv. Opt. Photon. **1**, 308 (2009).
10. M. T. Kauffman, W. C. Banyai, A. A. Godil, and D. M. Bloom, Appl. Phys. Lett. **64**, 270 (1994).
11. J. Azaña, Opt. Commun. **217**, 205 (2003).
12. J. Azaña, N. K. Berger, B. Levit, and B. Fischer, Appl. Opt. **43**, 483 (2004).
13. V. J. Hernandez, C. V. Bennett, B. D. Moran, A. D. Drobshoff, D. Chang, C. Langrock, M. M. Fejer, and M. Ibsen, Opt. Express **21**, 196 (2013).
14. B. H. Kolner and M. Nazarathy, Opt. Lett. **14**, 630 (1989).
15. B. H. Kolner, IEEE J. Quantum Electron. **30**, 1951 (1994).
16. C. V. Bennett and B. H. Kolner, Opt. Lett. **24**, 783 (1999).
17. R. Saperstein, N. Alić, D. Panasenko, R. Rokitski, and Y. Fainman, J. Opt. Soc. Am. B **22**, 2427 (2005).
18. M. A. Foster, R. Salem, Y. Okawachi, A. C. Turner-Foster, M. Lipson, and A. L. Gaeta, Nature **3**, 581 (2009).
19. X. Ribeyre, C. Rouyer, F. Raoult, D. Husson, C. Sauteret, and A. Migus, Opt. Lett. **26**, 1173 (2001).
20. R. Salem, M. A. Foster, and A. L. Gaeta, Adv. Opt. Photon. **5**, 274 (2013).
21. O. Martinez, IEEE J. Quantum Electron. **23**, 59 (1987).
22. E. Treacy, IEEE J. Quantum Electron. **5**, 454 (1969).
23. H. Luo, L. Qian, P. Yuan, and H. Zhu, Opt. Express **14**, 10631 (2006).
24. B. Afeyan, "STUD Pulses: Spike Train of Uneven Duration and Delay for the Control of Laser-Plasma Instabilities in ICF, IFE and HEDLP," BAPS DPP **TO5.7** (2009).
25. B. J. Albright, L. Yin, and B. Afeyan, Phys. Rev. Lett. **113**, 045002 (2014).
26. J. Meijer, K. Du, A. Gillner, D. Hoffmann, V. Kovalenko, T. Masuzawa, A. Ostendorf, R. Poprawe, and W. Schulz, CIRP Ann. **51**, 531 (2002).
27. C. Daniel, J. Full, L. González, C. Lupulescu, J. Manz, A. Merli, Š. Vajda, and L. Wöste, Science. **299**, 536 (2003).
28. C. H. Sarantos and J. E. Heebner, Opt. Lett. **35**, 1389 (2010).
29. R. Muir and J. Heebner, Opt. Lett. **42**, 4414 (2017).